2014

Variational Formulation of Macroparticle Models for Electromagnetic Plasma Simulations

Alexander B. Stamm
University of Nebraska-Lincoln, alexstamm@gmail.com

Bradley Allan Shadwick
University of Nebraska-Lincoln, shadwick@unl.edu

Evstati Georgiev Evstatiev
FAR-TECH, Inc., San Diego, CA, evstati@physics.utexas.edu

Pages: 1747 - 1758, DOI: 10.1109/TPS.2014.2320461

Variational Formulation of Macroparticle Models for Electromagnetic Plasma Simulations

Alexander B. Stamm, *Student Member, IEEE*, Bradley A. Shadwick, and Evstati G. Evstatiev

***Abstract*— A variational method is used to derive a self-consistent macroparticle model for relativistic electromagnetic kinetic plasma simulations. Extending earlier work, discretization of the electromagnetic Low Lagrangian is performed via a reduction of the phase-space distribution function onto a collection of finite-sized macroparticles of arbitrary shape and discretization of field quantities onto a spatial grid. This approach may be used with lab frame coordinates or moving window coordinates; the latter can greatly improve computational efficiency for studying some types of laser-plasma interactions. The primary advantage of the variational approach is the preservation of Lagrangian symmetries, which in our case leads to energy conservation and thus avoids difficulties with grid heating. In addition, this approach decouples particle size from grid spacing and relaxes restrictions on particle shape, leading to low numerical noise. The variational approach also guarantees consistent approximations in the equations of motion and is amenable to higher order methods in both space and time. We restrict our attention to the 1.5-D case (one coordinate and two momenta). Simulations are performed with the new models and demonstrate energy conservation and low noise.**

***Index Terms*— Electromagnetic, energy conserving, kinetic, particle in cell (PIC), plasma, variational.**

I. Introduction

COMPUTATION plays an indispensable role in contemporary plasma physics research. The dominant computational method is the particle-in-cell (PIC) method [1]–[3]. The computational efficiency and intuitive nature of the PIC method are largely responsible for this longevity. The PIC method is ubiquitous and its use routine owing to the ready availability of powerful computer systems. The computational demands of the PIC method strongly depend on system size and dimensionality. One-dimensional simulations can be readily performed on a modern laptop computer, while 3-D studies can require thousands of CPU cores and hundreds of thousands of CPU hours [4]. Despite the popularity of the PIC method, its theoretical underpinnings have been developed in a largely *ad hoc* manner by direct approximation of the equations of motion. For systems governed by variational principles—such as collisionless plasmas—it is well known that approximations performed at the level of the equation of motion risk the introduction of anomalous behavior, especially in the system invariants. In general, this is due to such approximations breaking the link between the resulting equations and the underlying variational principle. Indeed, the PIC method suffers from a number of unphysical artifacts [5]–[7]. While in some cases, empirical methods exist to suppress the unwanted behavior, the presence of these artifacts can greatly complicate interpretation of computational results [7].

Recently, a general class of macroparticle methods have been developed [8], [9] using a variational formulation based on Low's Lagrangian [10]. Significantly, this approach retains the connection between invariants and symmetries through Noether's theorem [11]. One immediate consequence of this connection is the absence of grid heating in these models [8]. Furthermore, this formulation allows for constructing models of arbitrary spatial and temporal order. In contrast, the overall accuracy of the usual PIC algorithm is at most second due to the nature of the force interpolation between the gridded field quantities and the (continuous) particle position. Again in contrast to the usual PIC algorithm, here the macroparticle shape is arbitrary; the spatial extent is completely decoupled from both the grid size and the smoothness of the shape; smoother particle shapes are not necessarily larger.

Here, we extend the original electrostatic analysis [8] to the simplest relativistic electromagnetic system suitable for the study of laser-plasma interactions, the so-called 1.5-D case. We retain a single spatial dimension (the laser propagation direction), z, and two particle momenta: one in the direction of the laser polarization, x, and other in the propagation direction. Taking the vector potential to be $\boldsymbol{A}$, we adopt the gauge fixing condition $\nabla \cdot \boldsymbol{A} = 0$, which, due to our geometry, reduces to $\partial A_z/\partial z = 0$. In an infinite domain, this implies $A_z = 0$. However, in a bounded domain, this condition allows $A_z = f(t)$, where $f(t)$ is determined by Ampere's law. For the examples we consider, A_z results in a small correction to the electric field, which we ignore for simplicity. In the 3-D case, choosing a particular gauge can be rather complicated as the typical gauge-fixing conditions lead to constrained variations; this is a subject of ongoing research and will be discussed in a future publication.

Our analysis is carried out with time treated as a continuous variable, and thus our equations of motion will be expressed as ordinary differential equations in t; it is in this continuous-time setting that conservations laws (resulting from symmetries in the Lagrangian) hold. Of course, to perform computations

Manuscript received September 25, 2013; revised March 25, 2014; accepted April 15, 2014. Date of current version June 6, 2014. This work was supported in part by the U.S. DoE under Contract DE-FG02-08ER55000 and Contract DE-SC0008382 and in part by the U.S. Department of Education under Grant P200A090156 GAANN.

A. B. Stamm and B. A. Shadwick are with the Department of Physics and Astronomy, University of Nebraska-Lincoln, Lincoln, NE 68588-0299 USA (e-mail: alexstamm@gmail.com; shadwick@unl.edu).

E. G. Evstatiev is with FAR-TECH, Inc., San Diego, CA 92121 USA (e-mail: evstati@physics.utexas.edu).

Color versions of one or more of the figures in this paper are available online at http://ieeexplore.ieee.org.

Digital Object Identifier 10.1109/TPS.2014.2320461

with these models, it will be necessary to make time discrete and, generically, conservation laws will only be preserved asymptotically to some order in the time-step, consistent with the accuracy of the integration method. There appears to be no impediment to constructing integrators for our models that respect conservation laws to machine precision, say, using the methods of [12]. Recently, implicit methods have been developed that yield exact energy conservation in the discrete-time case [13]–[15]. While these methods formally exactly conserve energy, in practice, the level of energy conservation achieved is determined by the accuracy with which a large nonlinear system of equations can be solved. Even when computational limitations preclude energy conservation to machine precision, these methods are free of grid heating and yield energy behavior superior to the traditional PIC methods. Here, we consider only generic integration methods and examine energy conservation in detail in Section II-C3. Developing integrators to exactly conserve energy for our models is a subject of active research by the authors and will be reported upon in due course.

In general, we adopt the conventions of [8]. We frame our discussion assuming dynamic electrons and immobile ions; generalization to the multispecies case is entirely straightforward. We reduce the distribution function to a collection of macroparticles, and to be concise, we proceed directly to represent the potentials using a spatial grid. While we only present a Lagrangian formulation, as in the electrostatic case [8], a noncanonical Hamiltonian [16], [17] formulation is also possible. We will report on the full 3-D case along with the Hamiltonian formulation in a forthcoming publication.

II. Reduction to Macroparticles and Gridded Fields

It has long been known that the Vlasov equation can be obtained from an action principle [10], [18], [19]. Given our geometry, the relativistic version of the Low Lagrangian [10] takes the form

$$\begin{aligned}\mathcal{L} = &\int d\tilde{z}\, d\tilde{v}_x\, d\tilde{v}_z\; f_0(\tilde{z},\tilde{v}_x,\tilde{v}_z)\\ &\times\left[-mc^2\sqrt{1-\frac{v_x^2}{c^2}-\frac{v_z^2}{c^2}}-q\,\varphi\,(z,t)+\frac{q}{c}\,v_x\,A_x\,(z,t)\right]\\ &+\frac{1}{8\pi}\int dz\left[\frac{1}{c^2}\left(\frac{\partial A_x}{\partial t}\right)^2-\left(\frac{\partial A_x}{\partial z}\right)^2+\left(\frac{\partial\varphi}{\partial z}\right)^2\right]\\ &-q_{\mathrm{I}}\int dz\, n^{(\mathrm{ION})}(z)\,\varphi(z,t)\end{aligned}\tag{1}$$

where $z(t;\tilde{z},\tilde{v}_x,\tilde{v}_z)$ and $v_x(t;\tilde{z},\tilde{v}_x,\tilde{v}_z)$ and $v_z(t;\tilde{z},\tilde{v}_x,\tilde{v}_z)$ are the electron position and components of velocity having initial conditions $z(0;\tilde{z},\tilde{v}_x,\tilde{v}_z)=\tilde{z}$, $v_x(0;\tilde{z},\tilde{v}_x,\tilde{v}_z)=\tilde{v}_x$ and $v_z(0;\tilde{z},\tilde{v}_x,\tilde{v}_z)=\tilde{v}_z$, $f_0(\tilde{z},\tilde{v}_x,\tilde{v}_z)$ is the initial electron phase space distribution, φ is the scalar potential, q and m are the electron charge and mass, respectively, q_{I} is the ion charge, $n^{(\mathrm{ION})}$ is a specified (nonevolving) ion density, and c is the speed of light. Since the ions are stationary their only contribution to the Lagrangian is their coupling to the electrostatic potential. Variations of the action obtained from (1) with respect to the particle positions yield the usual particle characteristic equations. Variation with respect to φ yields Poisson's equation with charge density

$$q\int dz\, dv_x\, dv_z\; f(z,v_x,v_z,t)+q_{\mathrm{I}}\,n^{(\mathrm{ION})}\tag{2}$$

while variation with respect to A_x yields Ampere's law with current

$$q\int dz\, dv_x\, dv_z\; f(z,v_x,v_z,t)\,v_x\,.\tag{3}$$

The evolution of the distribution function is obtained from $f(z,v_x,v_z,t)=f_0(\tilde{z},\tilde{v}_x,\tilde{v}_z)$, i.e., using the fact that the distribution function is constant along characteristics.

Following [8], we represent the phase space distribution function by a collection of macroparticles

$$f(z,v_x,v_z,t)=\sum_{\alpha=1}^{N_p}w_\alpha\, f_\alpha\tag{4}$$

where

$$f_\alpha = S[z-\xi_z^\alpha(t)]\,\delta[v_x-\dot{\xi}_x^\alpha(t)]\,\delta[v_z-\dot{\xi}_z^\alpha(t)],\tag{5}$$

w_α are constant weights, and the function S is the (fixed) spatial extent of the macroparticle, normalized as

$$\int dz\; S[z-\xi_z^\alpha(t)]=1.\tag{6}$$

Substituting our form of the distribution function into the Lagrangian and utilizing Gardner's restacking theorem [20], we obtain a reduced Lagrangian

$$\mathcal{L}=\mathcal{L}_{\mathrm{part}}+\mathcal{L}_{\mathrm{int}}+\mathcal{L}_{\mathrm{field}}+\mathcal{L}_{\mathrm{ion}}\tag{7}$$

where

$$\mathcal{L}_{\mathrm{part}}=-mc^2\sum_{\alpha=1}^{N_p}w_\alpha\sqrt{1-\frac{\dot{\xi}_x^{\alpha\,2}}{c^2}-\frac{\dot{\xi}_z^{\alpha\,2}}{c^2}}\tag{8}$$

$$\mathcal{L}_{\mathrm{int}}=-q\sum_{\alpha=1}^{N_p}w_\alpha\int dz\; S(z-\xi_z^\alpha)\left[\varphi(z,t)-\frac{\dot{\xi}_x^\alpha}{c}\,A(z,t)\right]\tag{9}$$

$$\mathcal{L}_{\mathrm{field}}=\frac{1}{8\pi}\int dz\,\left(\frac{1}{c^2}\,\dot{A}_x^2+A_x\frac{\partial^2 A_x}{\partial z^2}-\varphi\,\frac{\partial^2\varphi}{\partial z^2}\right)\tag{10}$$

$$\mathcal{L}_{\mathrm{ion}}=-q_{\mathrm{I}}\int dz\, n^{(\mathrm{ION})}(z)\,\varphi(z,t).\tag{11}$$

We have integrated by parts in the last two terms of $\mathcal{L}_{\mathrm{field}}$; as we will see below, the motivation for doing so lies with the finite difference expressions appearing in the discrete form of the field equations.

We now introduce a fixed (uniform) spatial grid z_i, $i\in[1,N_g]$ with grid spacing Δz and take $\varphi_i(t)$ and $A_i(t)$ to be the numerical approximation of $\varphi(z_i,t)$ and $A_x(z_i,t)$, respectively. As the particles positions are not constrained to coincide with the grid, some form of interpolation is required to approximate the potentials between grid points. Finite elements [21] offer a consistent way to perform such interpolations to any accuracy. Let $\Psi_i(z)$, $i=1,\ldots,N_g$ be a

finite-element basis of some order. We interpolate φ and A_x between the grid points by

$$\varphi(z,t) = \sum_{i=1}^{N_g} \varphi_i(t)\Psi_i(z) \quad \text{and} \quad A_x(z,t) = \sum_{i=1}^{N_g} A_i(t)\Psi_i(z)\,. \tag{12}$$

Thus

$$\begin{aligned}\int dz\, S(z-\xi_z^\alpha)\,\varphi(z,t) &= \sum_{i=1}^{N_g} \varphi_i \int dz\, S(z-\xi_z^\alpha)\,\Psi_i(z) \\ &= \sum_{i=1}^{N_g} \varphi_i\, \rho_i(\xi_z^\alpha)\end{aligned} \tag{13}$$

and likewise

$$\int dz\, S(z-\xi_z^\alpha)\, A_x(z,t) = \sum_{i=1}^{N_g} A_i\, \rho_i(\xi_z^\alpha) \tag{14}$$

where

$$\rho_i(\xi_z^\alpha) = \int dz\, S(z-\xi_z^\alpha)\,\Psi_i(z) \tag{15}$$

is the effective (projected) shape of the macroparticle. See [8, Table A.1] for explicit expressions for ρ_i for various shape functions, $S(z)$. Assuming that the $\Psi_i(z)$ are constructed from Lagrange polynomials, then $\sum_{i=1}^{N_g}\Psi_i(z) = 1$ and

$$\sum_{i=1}^{N_g} \rho_i(\xi^\alpha) = \sum_{i=1}^{N_g} \int dz\, S(z-\xi_z^\alpha)\,\Psi_i(z) = \int dz\, S(z-\xi_z^\alpha) = 1\,. \tag{16}$$

This means that at any instant, the total charge deposited on the grid is $q\sum_{\alpha=1}^{N_p} w_\alpha$ and the total transverse current is $q\sum_{\alpha=1}^{N_p} w_\alpha\,\dot{\xi}_x^\alpha$ (likewise the total longitudinal current is $q\sum_{\alpha=1}^{N_p} w_\alpha\,\dot{\xi}_z^\alpha$, but in our geometry, this current does not give rise to electromagnetic fields; its effects are contained within Poisson's equation). That is, at any instant, all of the charge and current associated with the macroparticles are accounted for on the grid.

The interaction terms (9) and (11) can now be written as

$$\mathcal{L}_{\text{int}} = -q\sum_{\alpha=1}^{N_p} w_\alpha \sum_{i=1}^{N_g}\left(\varphi_i - \frac{\dot{\xi}_x^\alpha}{c}A_i\right)\rho_i(\xi_z^\alpha) \tag{17}$$

and

$$\mathcal{L}_{\text{ion}} = -q_{\text{I}}\sum_{i=1}^{N_g} n_i^{(\text{ION})}\varphi_i\,. \tag{18}$$

Furthermore, we approximate the field terms (10) by expressing the spatial derivatives using finite differences and replacing the integral by a sum over grid points. Let K_{ij} be a finite difference analogue of $\partial^2/\partial z^2$, accurate to some order. We can then write the field Lagrangian as

$$\mathcal{L}_{\text{field}} = \frac{\Delta z}{8\pi c^2}\sum_{i=1}^{N_g}\dot{A}_i^2 + \frac{\Delta z}{8\pi}\sum_{i,j=1}^{N_g}\left(A_i\,K_{ij}\,A_j - \varphi_i K_{ij}\varphi_j\right). \tag{19}$$

Note that only the symmetric part of K_{ij} contributes to the Lagrangian. This has the effect of forcing K_{ij} to correspond to a central difference. Interestingly, nothing prevents the use of different finite-difference approximations for the scalar and vector potential terms, and thus it is possible to use separate grids for the potentials. For instance, in the case of under-dense laser-plasma interactions, the vector and scalar potentials can have very different resolution requirements: the vector potential, representing the laser, demands high resolution, while the scalar potential, representing the plasma response, can be adequately resolved with lower resolution. Hence, using separate grids may lead to improved computational performance.

A. Equation of Motion

The equations of motion are obtained from (7) by requiring the corresponding action to be stationary under variations of the particle position and the potentials. For the particles, the usual Euler–Lagrange equations

$$\frac{d}{dt}\frac{\partial\mathcal{L}}{\partial\dot{\xi}_{x,z}^\alpha} - \frac{\partial\mathcal{L}}{\partial\xi_{x,z}^\alpha} = 0 \tag{20}$$

give

$$\dot{\pi}_x^\alpha = -\frac{q}{c}\sum_{i=1}^{N_g}\frac{d}{dt}\left[A_i\,\rho_i(\xi_z^\alpha)\right] \tag{21}$$

$$= -q\sum_{i=1}^{N_g}\left[\frac{1}{c}\dot{A}_i\,\rho_i(\xi_z^\alpha) + \frac{\dot{\xi}_z^\alpha}{c}A_i\,\frac{\partial\rho_i(\xi_z^\alpha)}{\partial\xi_z^\alpha}\right] \tag{22}$$

and

$$\dot{\pi}_z^\alpha = -q\sum_{i=1}^{N_g}\frac{\partial\rho_i(\xi_z^\alpha)}{\partial\xi_z^\alpha}\left(\varphi_i - \frac{\dot{\xi}_x^\alpha}{c}A_i\right) \tag{23}$$

where $\pi_x^\alpha \equiv m\,\gamma_\alpha\,\dot{\xi}_x^\alpha$ and $\pi_z^\alpha \equiv m\,\gamma_\alpha\,\dot{\xi}_z^\alpha$ are the usual relativistic particle momenta with

$$\gamma_\alpha = \sqrt{1 + \frac{\pi_x^{\alpha\,2}}{m^2c^2} + \frac{\pi_z^{\alpha\,2}}{m^2c^2}}\,. \tag{24}$$

Note that ξ_x^α is a cyclic variable, and (21) is just a statement of conservation of transverse canonical momentum. It turns out that the numerical implementation is simpler and the energy conservation properties (see below) are better if we evolve π_x^α according to (22) in preference to using the conservation law (21). These evolution equations correspond to the Lorentz force; however, the discretization has the effect of moving the derivative that would act on the potentials in the continuous case to act instead on the particle shape. In essence, an integration by parts is performed behind the scenes.

The Euler–Lagrange equation for the scalar potential is simply $\partial\mathcal{L}/\partial\varphi_i = 0$, giving

$$\sum_{j=1}^{N_g} K_{ij}\varphi_j = -\frac{4\pi}{\Delta z}\left[q\sum_{\alpha=1}^{N_p} w_\alpha\,\rho_i(\xi_z^\alpha) + q_{\text{I}}\,n_i^{(\text{ION})}\right] \tag{25}$$

which is the discretized form of Poisson's equation. Similarly, the Euler–Lagrange equation for the vector potential is

$$\frac{d}{dt}\left(\frac{\partial\mathcal{L}}{\partial\dot{A}_i}\right) - \frac{\partial\mathcal{L}}{\partial A_i} = 0 \tag{26}$$

leading to the wave equation

$$\ddot{A}_i - c^2 \sum_{j=1}^{N_g} K_{ij} A_j = \frac{4\pi q c}{\Delta z} \sum_{\alpha=1}^{N_p} w_\alpha \dot{\xi}_x^\alpha \rho_i(\xi_z^\alpha) . \tag{27}$$

The consequence of integrating by parts in the field terms in the Lagrangian can now be made clear. Since the terms for both A_x and φ have the same structure, it suffices to consider only φ. Suppose we had not integrated by parts and had introduced different finite-difference representations for each factor of $\partial\varphi/\partial z$ in the Lagrangian, writing

$$\frac{1}{8\pi}\int dz \left(\frac{\partial\varphi}{\partial z}\right)^2 \approx \frac{\Delta z}{4\pi} \sum_{k,l,m=1}^{N_g} \frac{1}{2}\left(D_{kl}^{(1)}\varphi_l \, D_{km}^{(2)}\varphi_m\right) \tag{28}$$

where $D_{ij}^{(1,2)}\varphi_j$ is any finite-difference approximation to $\partial\varphi/\partial z$ at z_i. Differentiating with respect to φ_i (as is done to obtain the equation of motion), we have

$$\begin{aligned}\frac{1}{2}&\left(D_{ki}^{(1)} D_{km}^{(2)}\varphi_m + D_{kl}^{(1)}\varphi_l D_{ki}^{(2)}\right) \\ &= \frac{1}{2}\left(D_{ki}^{(1)} D_{kj}^{(2)} + D_{ki}^{(2)} D_{kj}^{(1)}\right)\varphi_j \\ &= \frac{1}{2}\left(D^{(1)T} D^{(2)} + D^{(2)T} D^{(1)}\right)_{ij}\varphi_j \\ &= \widetilde{K}_{ij}\varphi_j . \end{aligned} \tag{29}$$

Regardless of the details of $D^{(1)}$ and $D^{(2)}$, $\widetilde{K}$ is symmetric, i.e., $\widetilde{K}$ corresponds to some central difference. Thus, whether one integrates by parts in the Lagrangian or not, the spatial difference operators in the wave equation and Poisson's equation always correspond to some form of central differencing. Performing the integration by parts as we have done leading up to (19) allows one to directly specify the difference operator ultimately appearing in the field equations. This is particularly important with regard to the wave equation as it is hyperbolic and numerical stability [22] will have to be considered. For example, suppose we take $D^{(1)} = D^{(2)} = D$ to correspond to second-order central differences $D_{ij} = (\delta_{i+1,j} - \delta_{i-1,j})/(2\Delta z)$, where $\delta_{i,j}$ is the Kronecker delta, then $\widetilde{K}$ (up to a sign) corresponds to the standard second-order central difference for the second derivative but with twice the grid spacing:

$$\begin{aligned}\frac{1}{2}&\left(D_{ki}^{(1)} D_{kj}^{(2)} + D_{ki}^{(2)} D_{kj}^{(1)}\right) = D_{ki}\, D_{kj} \\ &= \frac{1}{(2\Delta z)^2}\left(\delta_{k+1,i} - \delta_{k-1,i}\right)\left(\delta_{k+1,j} - \delta_{k-1,j}\right) \\ &= \frac{1}{(2\Delta z)^2}\left(\delta_{k+1,i}\,\delta_{k+1,j} - \delta_{k+1,i}\,\delta_{k-1,j}\right. \\ &\qquad \left. -\delta_{k-1,i}\,\delta_{k+1,j} + \delta_{k-1,i}\,\delta_{k-1,j}\right) \\ &= -\frac{1}{(2\Delta z)^2}\left(\delta_{i+2,j} - 2\,\delta_{i,j} + \delta_{i-2,j}\right). \end{aligned} \tag{30}$$

Here, the sign change is the same as occurs under integration by parts.

B. Energy Conservation

Since our Lagrangian has no explicit time dependence, we will have a conserved energy, W, which can be obtained from the Lagrangian in the usual way:

$$W = \sum_{\alpha=1}^{N_p}\left(\dot{\xi}_x^\alpha \frac{\partial\mathcal{L}}{\partial\dot{\xi}_x^\alpha} + \dot{\xi}_z^\alpha \frac{\partial\mathcal{L}}{\partial\dot{\xi}_z^\alpha}\right) + \sum_{i=1}^{N_g}\dot{A}_i \frac{\partial\mathcal{L}}{\partial\dot{A}_i} - \mathcal{L} . \tag{31}$$

Evaluating W with the discretized Lagrangian, we obtain

$$\begin{aligned} W = {} & mc^2 \sum_{\alpha=1}^{N_p} w_\alpha \gamma_\alpha + q\sum_{\alpha=1}^{N_p}\sum_{i=1}^{N_g} w_\alpha \varphi_i \rho_i(\xi_z^\alpha) \\ & + q_{\mathrm{I}} \sum_{i=1}^{N_g} n_i^{(\mathrm{ION})}\varphi_i + \frac{\Delta z}{8\pi c^2}\sum_{i=1}^{N_g}\dot{A}_i^2 \\ & + \frac{\Delta z}{8\pi}\sum_{i,j=1}^{N_g}\left(\varphi_i K_{ij}\varphi_j - A_i K_{ij} A_j\right) . \end{aligned} \tag{32}$$

Using the discrete form of Poisson's equation (25), we can write the energy in the more recognizable form

$$\begin{aligned} W = {} & mc^2 \sum_{\alpha=1}^{N_p} w_\alpha \gamma_\alpha + \frac{\Delta z}{8\pi c^2}\sum_{i=1}^{N_g}\dot{A}_i^2 \\ & - \frac{\Delta z}{8\pi}\sum_{i,j=1}^{N_g}\left(\varphi_i K_{ij}\varphi_j + A_i K_{ij} A_j\right) \end{aligned} \tag{33}$$

where the first term is the kinetic energy of the particles and the remaining terms give the discrete representation of the field energy. Using the equations of motion, it is straightforward to show that W is an invariant

$$\begin{aligned} \frac{dW}{dt} = {} & mc^2 \sum_{\alpha=1}^{N_p} w_\alpha \frac{d\gamma_\alpha}{dt} + \frac{\Delta z}{4\pi c^2}\sum_{i=1}^{N_g}\dot{A}_i\,\ddot{A}_i \\ & - \frac{\Delta z}{4\pi}\sum_{i,j=1}^{N_g}\left(\varphi_i K_{ij}\dot{\varphi}_j + \dot{A}_i K_{ij} A_j\right) \\ = {} & mc^2 \sum_{\alpha=1}^{N_p} w_\alpha \left(\frac{\partial\gamma_\alpha}{\partial\pi_x^\alpha}\frac{d\pi_x^\alpha}{dt} + \frac{\partial\gamma_\alpha}{\partial\pi_z^\alpha}\frac{d\pi_z^\alpha}{dt}\right) \\ & + \frac{q}{c}\sum_{i=1}^{N_g}\dot{A}_i \sum_{\alpha=1}^{N_p} w_\alpha \dot{\xi}_x^\alpha \rho_i - \frac{\Delta z}{4\pi}\sum_{i,j=1}^{N_g}\varphi_i K_{ij}\dot{\varphi}_j \end{aligned} \tag{34}$$

where we have used (27). From (24), we find $mc^2\partial\gamma_\alpha/\partial\pi_{x,z}^\alpha = \dot{\xi}_{x,z}^\alpha$. In addition, we obtain $\dot{\varphi}_j$ from the time derivative of (25). Together these give

$$\begin{aligned} \frac{dW}{dt} = {} & \sum_{\alpha=1}^{N_p} w_\alpha \left(\dot{\xi}_x^\alpha \dot{\pi}_x^\alpha + \dot{\xi}_z^\alpha \dot{\pi}_z^\alpha\right) \\ & + q\sum_{\alpha=1}^{N_p} w_\alpha \sum_{i=1}^{N_g}\left(\frac{\dot{\xi}_x^\alpha}{c}\dot{A}_i \rho_i + \varphi_i \frac{d\rho_i}{dt}\right) \\ = {} & 0 \end{aligned} \tag{35}$$

where the last step follows from the macroparticle equations of motion (22) and (23).

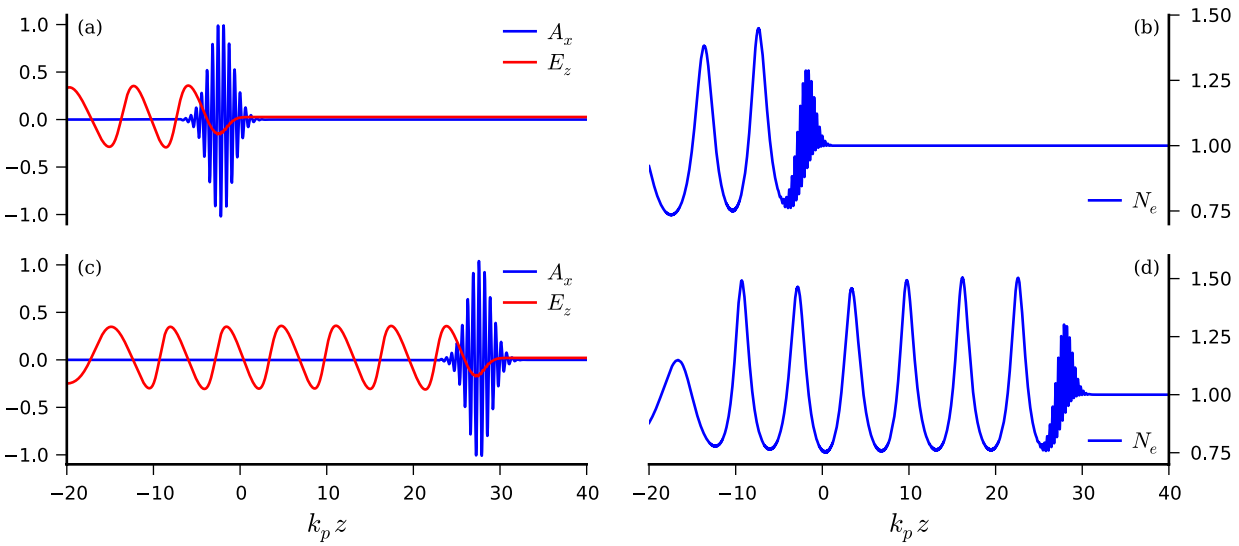

Fig. 1. Laser pulse interacting with an under-dense plasma at $\omega_p t = 50$ [(a) and (b)] and $\omega_p t = 80$ [(c) and (d)]. Shown in (a) and (c) are $q A_x/mc^2$ (red) and $q E_z/mc\omega_p$ (blue). Shown in (b) and (d) is N_e/n_0.

C. Examples

Throughout we have treated time as a continuous variable; nonetheless, a numerical solution of the equations of motion necessarily requires discretizing in time. Our formalism is indifferent to the method used to integrate the equations of motion. Indeed, it is a significant advantage of our approach that the spatial and temporal discretizations are fully decoupled. The choice of spatial differencing (which enters through K_{ij}) essentially determines which temporal discretizations will be stable [22]. Thus, the absolute freedom to choose the temporal integration scheme ensures that numerically stable algorithms can be constructed. We consider two different time integration methods. For simplicity, in both cases, we adopt second-order finite differences in space and linear finite elements, $\Psi_i(z)$, for interpolation (also accurate to second order). This interpolation scheme is the same as used in [8]. Empirically, we find that numerical stability of this system is dominated by the free space behavior of the wave equation. A simple stability analysis of the wave equation shows that, with the second-order central differencing in space, second order, explicit time integration is unconditionally unstable [23]. While both third- and fourth-order methods are stable, the stability limit for the fourth order is larger [23]. This leads us to choose a fixed-step fourth-order Runge–Kutta scheme [24]; in the following, we will refer to this as RK4.

Alternatively, the Crank–Nicholson scheme [25] is unconditionally stable for the wave equation. To avoid a fully implicit solution of the equations of motion, we use Strang-style operator splitting [26], solving the particle equations (including Poisson's equation) with fixed fields and the wave equation with fixed current. We use a second-order Runge–Kutta method for the particles (we could have just as well used Milne's method [27], but it requires more intermediate storage) and the Crank–Nicolson method for the fields. The Crank–Nicolson method for the wave equation is also implicit but leads to a bi–tridiagonal system of linear equations for which a fast direct method exists [28]. Since the field solve is much less computational effort than the particle advance, we choose to perform a half time-step field solve, followed by a full time-step evolution of the particles and electrostatic potential and a final half time-step field solve. Subsequently, we refer to this method as RK2-Split.

Our examples consist of a laser pulse incident on an initially quiescent plasma slab. We consider two cases: 1) $\omega_0 = 10\,\omega_p$ (the under-dense case) and 2) $\omega_0 = \omega_p$ (the over-dense case), where ω_0 is the initial laser frequency and $\omega_p = \sqrt{4\pi\, q^2 n_0/m}$ is the plasma frequency with n_0 the ambient plasma density. The initial vector potential is given by

$$A_x = a_0 \frac{mc^2}{q} \exp\left[-\left(\frac{z - z_0}{L}\right)^2\right] \cos\left[k_0 (z - z_0)\right] \qquad (36)$$

where $k_0 = \omega_0/c$ is the initial laser wave number, z_0 is the initial location of the center of the pulse, and L is the pulse length. Initially, $\partial A_x/\partial t$ is chosen to correspond to a forward propagating pulse. We impose conducting boundary conditions, taking both $\varphi = 0$ and $A_x = 0$ at the boundary. The computational grid extends from z_1 to z_2 and corresponds to the interior of the problem domain, i.e., the boundary conditions are applied at $z_1 - \Delta z$ and $z_2 + \Delta z$. The ion density profile varies from vacuum to a uniform plateau of density n_0 as a linear ramp with quadratically rounded corners. At the center of the transition z_r, the ramp has slope $2n_0/L_r$; the entire transition has length L_r. Macroparticles are loaded at rest with variable weights to give a charge-neutral initial density. All computations are done in dimensionless form with length and time-scales determined by $k_p = \omega_p/c$ and ω_p, respectively; momenta are normalized to mc, and potentials to mc^2/q.

1) Under-Dense Case: Here, we take $\omega_0 = 10\,\omega_p$, $a_0 = 1$, $k_p L = 2$, $k_p z_0 = -50$, $k_p z_1 = -60$, $k_p z_2 = 90$, $k_p L_r = 40$, and $k_p z_r = -30$, and we use one macroparticle per cell. The long ramp was chosen to minimize particle trapping at the vacuum–plasma interface. This problem is solved over a range of grid parameters and with both the RK2-Split and

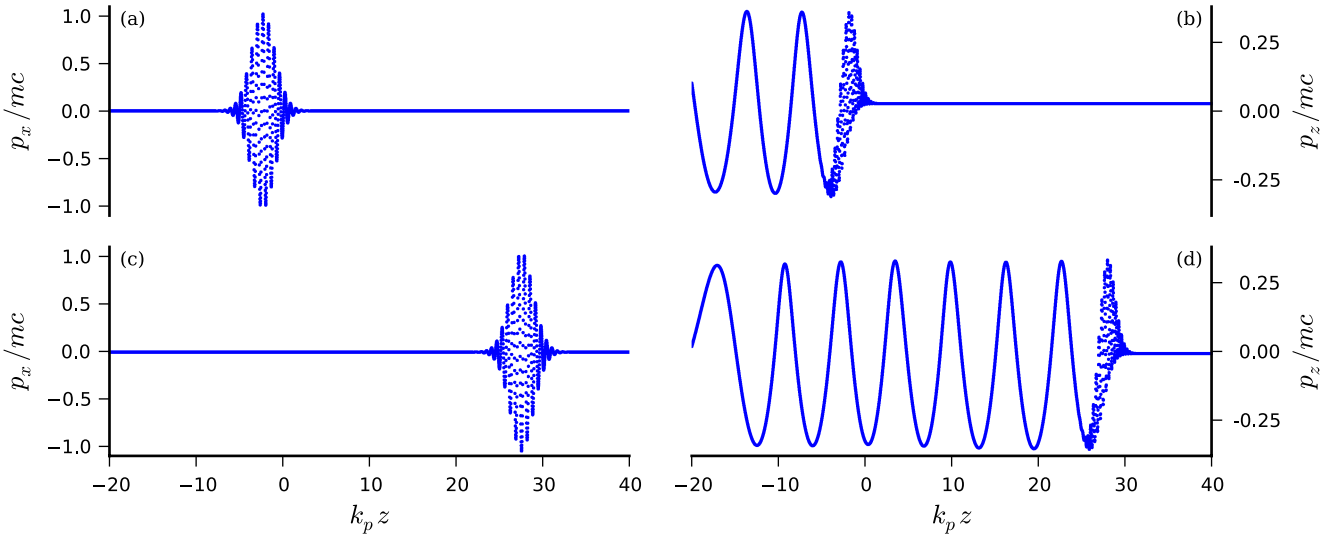

Fig. 2. Macroparticle phase space resulting from the interaction of a laser pulse with an under-dense plasma at $\omega_p t = 50$ [(a) and (b)] and $\omega_p t = 80$ [(c) and (d)]. Shown in (a) and (c) is π_x^α/mc and in (b) and (d) is π_z^α/mc. Each dot corresponds to a single macroparticle.

RK4 methods; see below. Figs. 1 and 2 show the results with the highest resolution ($k_p\,\Delta z = 0.05$, corresponding to 12 001 grid points, and $c\,\Delta t = \Delta z/8$) and quartic ρ_k using the RK4 method at $\omega_p t = 50$ and $\omega_p t = 80$. See [8, Table A.1] for explicit expressions for the particle shapes and the ρ_k. In Fig. 1, we plot the dimensionless fields $q\,A_x/mc^2$, $q\,E_z/m\,c\,\omega_p$ [panels (a) and (c)], and N_e/n_0 [panels (b) and (d)]. We compute the longitudinal electric field E_z from the potential

$$E_z(z_i) = \frac{1}{2\Delta z}\,(\varphi_{i-1} - \varphi_{i+1}) \tag{37}$$

and define the macroparticle density on the grid, N_e, based on the right-hand side of Poisson's equation

$$N_e(z_i) = \sum_{\alpha=1}^{N_p} w_\alpha\,\rho_i(\xi_z^\alpha)\,. \tag{38}$$

In Fig. 2, we plot the dimensionless macroparticle momentum π_x^α/mc [Fig. 2(a) and (c)] and π_z^α/mc [Fig. 2(b) and (d)].

As can be seen in the figures, a clean and well-defined plasma wave is generated. It should be emphasized that neither the fields (including the density) nor the phase space have been smoothed in any way. As mentioned above, we choose to evolve π_x^α using (22) in place of the conservation law (21). Fig. 3 shows the transverse momentum overlaid on $-q\,A_x/c$ at $\omega_p t = 50$ and $\omega_p t = 80$. The spatial grid is sufficiently fine that A_x is nearly constant over the macroparticle, leading to $\pi_x^\alpha \approx -q\,A_x/c$ to a very good approximation, as can be seen in Fig. 3.

2) Over-Dense Case: Here, we take $\omega_0 = \omega_p$, $a_0 = 0.5$, $k_p L = 10$, $k_p z_0 = -40$, $k_p z_1 = -75$, $k_p z_2 = 75$, $k_p L_r = 15$, and $k_p z_r = 0$, and we use 10 macroparticles per cell. This problem is solved over a range of grid parameters and with both the RK2-Split and RK4 methods; see below. Fig. 4 shows the results with the highest resolution ($k_p\,\Delta z = 0.025$, corresponding to 6001 grid points, and $c\,\Delta t = \Delta z/9$)

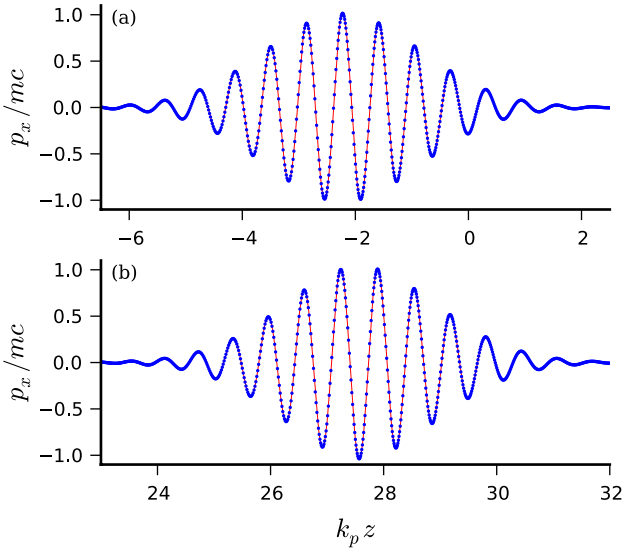

Fig. 3. Comparison of the macroparticle transverse momentum π_x^α/mc (blue dots) and $-q\,A_x/mc^2$ (red line) at (a) $\omega_p t = 50$ and (b) $\omega_p t = 80$.

and quartic ρ_k using the RK4 method. Plotted in Fig. 4 are $q\,A_x/mc^2$ and $J_x/q\,n_0$ on the left axis and N_e/n_0 on the right axis at $\omega_p t = 0$ [Fig. 4(a)], $\omega_p t = 50$ [Fig. 4(b)], and $\omega_p t = 100$ [Fig. 4(c)]. We define the transverse current on the grid, J_x, based on the right-hand side of the wave equation (27) as

$$J_x(z_i) = \frac{q}{\Delta z}\sum_{\alpha=1}^{N_p} w_\alpha\,\dot{\xi}_x^\alpha\,\rho_i(\xi_z^\alpha)\,. \tag{39}$$

As can be seen in the figure, the laser pulse is absorbed on the density transition, resulting in surface currents in the transition region [Fig. 4(b)], which subsequently reradiate a left-going pulse as well as an evanescent wave [Fig. 4(c)].

3) Energy Conservation: As we saw, the continuous-time equations of motion exactly conserve total energy. When these

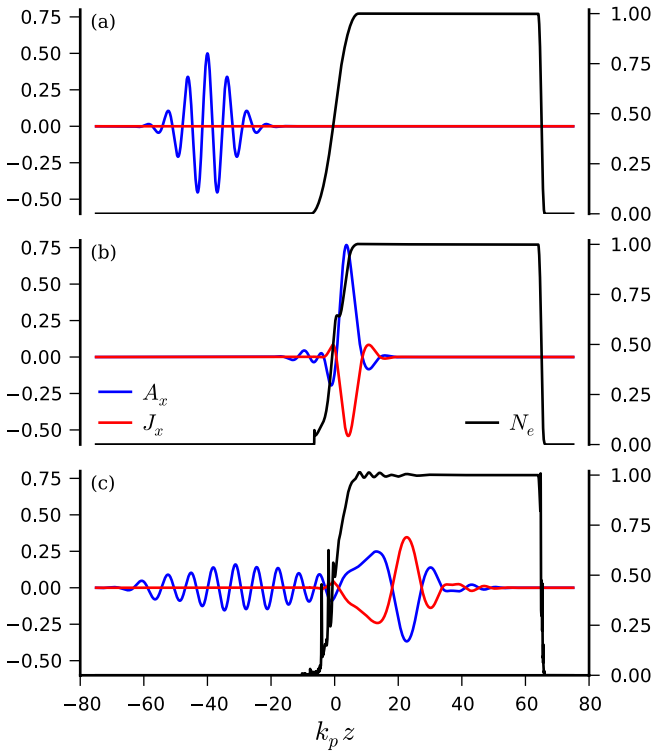

Fig. 4. Laser pulse interacting with an over-dense plasma at (a) $\omega_p t = 0$, (b) $\omega_p t = 50$, and (c) $\omega_p t = 100$. The vector potential $q A_x/mc^2$ (red line) and transverse current $J_x/q n_0$ (blue line) are plotted on the left axis, while the macroparticle density N_e/n_0 (black line) is plotted on the right axis. The density shows the vacuum-plasma interface.

equations are integrated numerically, we expect, as a consequence of the time discretization, that energy will no longer be exactly conserved. (It may be possible to construct special purpose integrators for these equations of motion that do exactly conserve energy [12].) However, since any departure from exact energy conservation is due solely to the temporal discretization, the resulting error in total energy should then only depend on Δt and should scale with Δt consistent with the order of accuracy of the temporal integration. This is in marked contrast to the usual PIC algorithm, where the energy error in general depends on both the time-step and the grid spacing.

To demonstrate this characteristic of the energy error, we solve both the under-dense and over-dense problems with each method for a collection of grid sizes and time-steps. Since the RK4 method has a stability limit, we set the largest time-step considered to $c\,\Delta t = \Delta z$; the actual stability threshold is $c\,\Delta t \leq \sqrt{2}\,\Delta z$ [23]. The RK2-Split method has a large stability basin; however, for $c\,\Delta t > \Delta z$, there is substantial dispersion in the field solver, and thus for accuracy reasons, we restrict $c\,\Delta t \leq \Delta z$ for this method as well.

In Figs. 5 and 6, we plot the relative energy error in the under-dense case for the RK2-Split and RK4 methods, respectively, with $k_p\,\Delta z$ ranging from 0.05 to 0.0125 and $c\,\Delta t = \Delta z$ to $c\,\Delta t = \Delta z/8$ for four particle shapes. In each figure, a scaling with Δt is plotted to aid the eye (blue line); the exponent is obtained by fitting the errors. Figs. 5(a) and 6(a) have fewer points than the other panels due to a technical detail of our implementations. To simplify our numerical implementations, we assume that no macroparticles leave the domain. If a macroparticle reaches the domain boundary, the computation is terminated. At lower resolution, several of the computations with linear ρ_k failed for this reason and are thus absent from the plots. For the RK2-Split method, we expect the energy error to scale with Δt^2 (consistent with the global error of the method). For all ρ_k except the linear case, we see nearly perfect power law scaling with Δt, with a rather larger exponent than expected. For linear ρ_k, the energy error shows some spread amongst the different spatial resolutions. Now, $\partial\rho_k/\partial t \propto \partial\rho_k/\partial\xi$ which, for linear particles, has a discontinuity whose size depends on Δz. As a result, the usual truncation error analysis does not hold (the numerical method is sampling this derivative and is sensitive to the discontinuity). For the RK4 method, we again see some spread for linear ρ_k and perhaps some (much smaller) spread for quadratic ρ_k. The quadratic ρ_k have discontinuities in their second derivative, which the RK4 method samples. (We expect to see this also in the cubic ρ_k but evidently the effect is too small to be observable.)

In Figs. 7 and 8, we plot the relative energy error in the over-dense case for the RK2-Split and RK4 methods, respectively, with $k_p\,\Delta z$ ranging from 0.4 to 0.025 and $c\,\Delta t = \Delta z$ to $c\,\Delta t = \Delta z/9$ for four particle shapes. In each figure, a scaling with Δt is plotted to aid the eye (blue line); the exponent is obtained by fitting the errors. Overall, the behavior is comparable with the under-dense case. For the RK4 method, the departure from the power-law scaling for linear ρ_k is more pronounced than in the under-dense case (whereas this departure is barely noticeable for the RK2-Split method). The scatter seen for $\omega_p\Delta t \lesssim 2 \times 10^{-2}$ is due to numerical precision. While all computations are done in double precision (≈15 digits), the results are stored to disk in single precision (≈8 digits). For $\omega_p\Delta t$ below this threshold, the stored solutions do not have sufficient precision to faithfully represent the system energy.

In no case, do we see any hint of grid heating; this is completely consistent with our formulation that exactly conserves energy even with the presence of a spatial grid.

III. Moving Window Formulation

A tremendous advantage of the Lagrangian formalism is that the Euler–Lagrange equations are form-invariant under arbitrary (invertible) point transformations of the dynamical variables. For some types of laser–plasma interactions, moving window coordinates (comoving with the laser pulse) can greatly reduce the computational cost of simulations. Here, we transform our macroparticle model to moving coordinates. While it might be more elegant to apply the transformation to the discrete systems, this is undesirable due to the time dependence in the transformation. Thus, we transform the continuous space macroparticle Lagrangian (7) to the moving window coordinates, and then discretize the fields.

In the moving window, our new coordinates ζ and τ are defined by $\zeta = c\,t - z$, $\tau = t$. Partial derivatives in the two coordinate systems are related by $\partial/\partial z = -\partial/\partial\zeta$ and

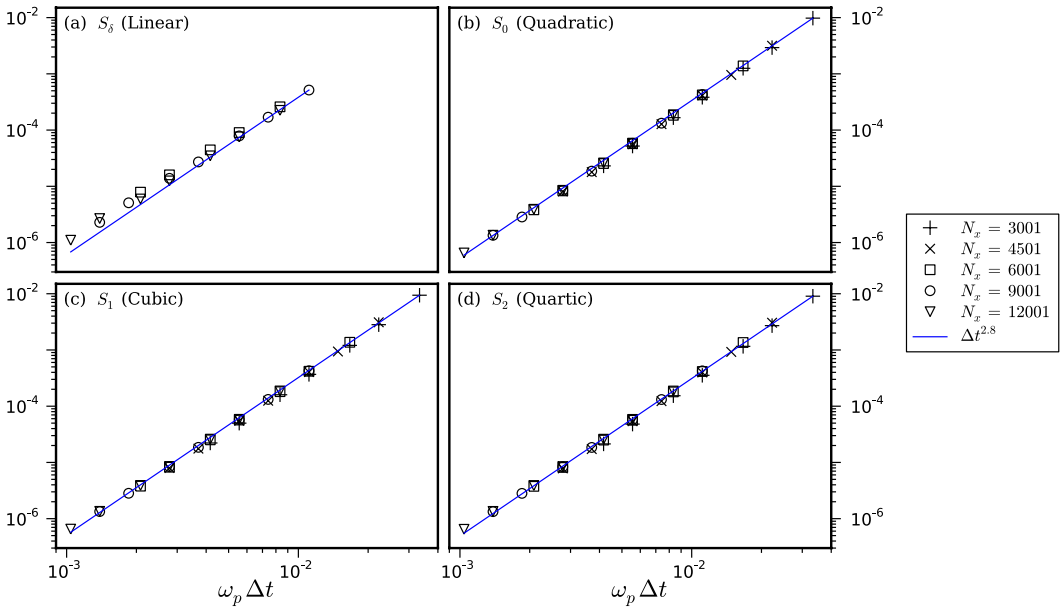

Fig. 5. Energy conservation in the under-dense case for the RK2-Split method. The relative energy error is shown as a function of Δt for various spatial resolutions and particle shapes. As expected, the energy error depends only on the temporal discretization. The panels are labeled with the particle shape S and the resulting order of ρ_k. The shapes are named following [8].

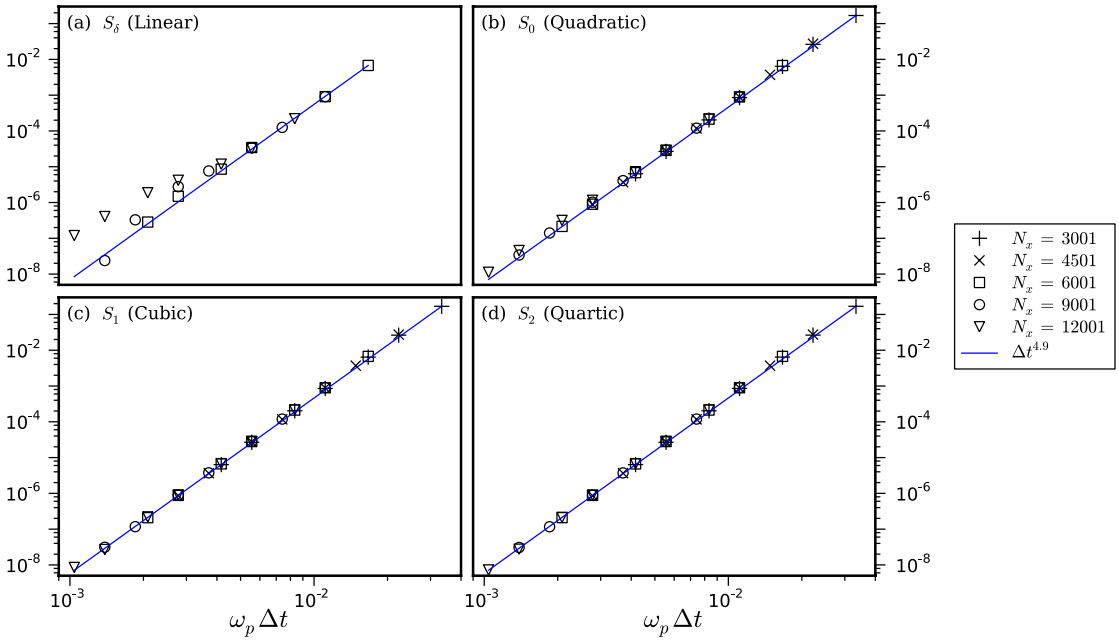

Fig. 6. Energy conservation in the under-dense case for the RK4 method. The relative energy error is shown as a function of Δt for various spatial resolutions and particle shapes. As expected, the energy error depends only on the temporal discretization. The panels are labeled with the particle shape S and the resulting order of ρ_k. The shapes are named following [8].

$\partial/\partial t = \partial/\partial\tau + c\,\partial/\partial\zeta$. The new particle positions and velocities become $\eta_z^\alpha = c\,t - \zeta_z^\alpha$, $\dot{\eta}_x^\alpha \equiv d\eta_x^\alpha/d\tau = \dot{\zeta}_x^\alpha$, and $\dot{\eta}_z^\alpha \equiv d\eta_z^\alpha/d\tau = c - \dot{\zeta}_z^\alpha$. Under this transformation, the Lagrangian becomes

$$\mathcal{L} = \mathcal{L}_{\text{part}} + \mathcal{L}_{\text{int}} + \mathcal{L}_{\text{field}} + \mathcal{L}_{\text{ion}} \tag{40}$$

where

$$\mathcal{L}_{\text{part}} = -mc^2 \sum_{\alpha=1}^{N_p} w_\alpha \sqrt{1 - \frac{\dot{\eta}_x^{\alpha\,2}}{c^2} - \left(1 - \frac{\dot{\eta}_z^\alpha}{c}\right)^2} \tag{41}$$

$$\mathcal{L}_{\text{int}} = -q \sum_{\alpha=1}^{N_p} w_\alpha \int d\zeta\; S(\eta_z^\alpha - \zeta)\left[\widetilde{\varphi}(\zeta,\tau) - \frac{\dot{\eta}_x^\alpha}{c}\,\widetilde{A}_x(\zeta,\tau)\right] \tag{42}$$

$$\mathcal{L}_{\text{field}} = \frac{1}{8\pi}\int d\zeta \left[\frac{1}{c^2}\left(\frac{\partial \widetilde{A}_x}{\partial \tau}\right)^2 + \frac{2}{c}\,\frac{\partial \widetilde{A}_x}{\partial \tau}\,\frac{\partial \widetilde{A}_x}{\partial \zeta} - \widetilde{\varphi}\,\frac{\partial^2 \widetilde{\varphi}}{\partial \zeta^2}\right] \tag{43}$$

$$\mathcal{L}_{\text{ion}} = -q_{\text{I}} \int d\zeta\; \widetilde{n}^{(\text{ION})}(\zeta,\tau)\,\widetilde{\varphi}(\zeta,\tau) \tag{44}$$

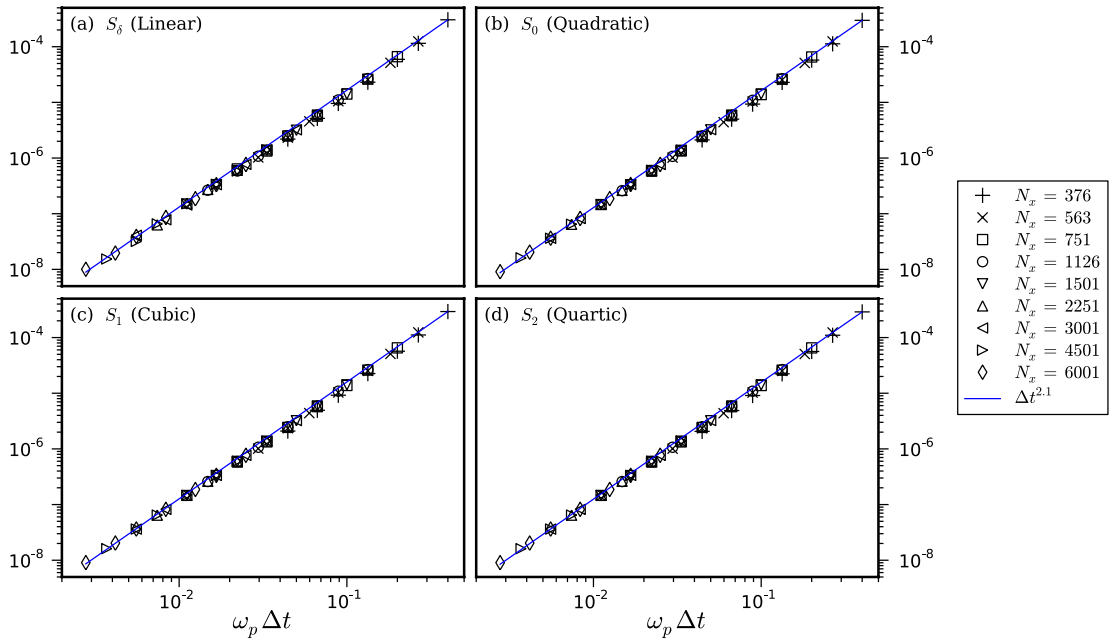

Fig. 7. Energy conservation in the over-dense case for the RK2-Split method. The relative energy error is shown as a function of Δt for various spatial resolutions and particle shapes. As expected, the energy error depends only on the temporal discretization. The panels are labeled with the particle shape S and the resulting order of ρ_k. The shapes are named following [8].

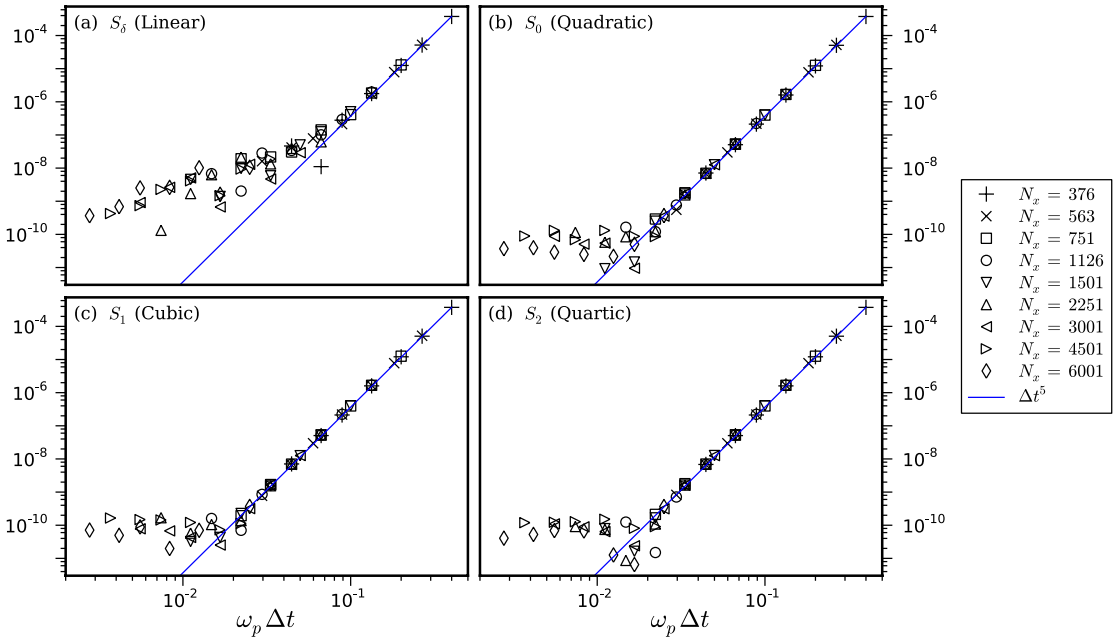

Fig. 8. Energy conservation in the over-dense case for the RK4 method. The relative energy error is shown as a function of Δt for various spatial resolutions and particle shapes. As expected, the energy error depends only on the temporal discretization. The panels are labeled with the particle shape S and the resulting order of ρ_k. The shapes are named following [8].

where $\widetilde{\varphi}(\zeta,\tau) = \varphi(z,t)$, $\widetilde{A}_x(\zeta,\tau) = A_x(z,t)$, and $\widetilde{n}^{(\mathrm{ION})}(\zeta,\tau) = n^{(\mathrm{ION})}(z,t)$. Note that spatial variation in the ion density leads to time dependence of $\widetilde{n}^{(\mathrm{ION})}$ in the moving window.

We discretize (41)–(44) by introducing a uniform grid ζ_i, $i \in [1, N_g]$, with spacing $\Delta\zeta$ and follow the procedure described in Section II. If the shape function $S(z)$ is symmetric, i.e., if $S(-z) = S(z)$ (there seems little motivation for S to be otherwise), then the projected particle shape ρ_k in the moving window is identical to that in the lab frame. The discrete analogs of (41)–(44) are found to be

$$\mathcal{L}_{\mathrm{part}} = -mc^2 \sum_{\alpha=1}^{N_p} w_\alpha \sqrt{1 - \frac{\dot{\eta}_x^{\alpha\,2}}{c^2} - \left(1 - \frac{\dot{\eta}_z^\alpha}{c}\right)^2} \tag{45}$$

$$\mathcal{L}_{\mathrm{int}} = -q \sum_{\alpha=1}^{N_p} w_\alpha \sum_{i=1}^{N_g} \left(\varphi_i - \frac{\dot{\eta}_x^\alpha}{c} A_i\right) \rho_i(\eta_z^\alpha) \tag{46}$$

$$\mathcal{L}_{\text{field}} = \frac{\Delta\zeta}{8\pi c^2}\sum_{i=1}^{N_g}\dot{A}_i^2 + \frac{\Delta\zeta}{4\pi c}\sum_{i,j=1}^{N_g}\dot{A}_i D_{ij} A_j - \frac{\Delta\zeta}{8\pi}\sum_{i,j=1}^{N_g}\varphi_i K_{ij}\varphi_j \quad (47)$$

and

$$\mathcal{L}_{\text{ion}} = -q_{\text{I}}\sum_{i=1}^{N_g} n_i^{(\text{ION})}\varphi_i \quad (48)$$

where $\varphi_i(\tau)$ and $A_i(\tau)$ are the numerical approximations to $\widetilde{\varphi}(\zeta_i,\tau)$ and $\widetilde{A}_x(\zeta_i,\tau)$, respectively.

The equations of motion are obtained in the usual way, giving

$$\dot{\pi}_x^\alpha = -\frac{q}{c}\sum_k \frac{d}{d\tau}\left[A_k\,\rho_k(\eta_z^\alpha)\right] \quad (49)$$

$$\dot{\pi}_z^\alpha = q\sum_k \frac{\partial\rho_k(\eta_z^\alpha)}{\partial\eta_z^\alpha}\left(\varphi_k - \frac{\dot{\eta}_x^\alpha}{c}A_k\right) \quad (50)$$

$$\sum_{j=1}^{N_g} K_{ij}\varphi_j = -\frac{4\pi}{\Delta\zeta}\left[q\sum_{\alpha=1}^{N_p} w_\alpha\,\rho_i(\eta_z^\alpha) + q_{\text{I}}\,n_i^{(\text{ION})}\right] \quad (51)$$

and

$$\ddot{A}_i + c\sum_{j=1}^{N_g}\left(D_{ij} - D_{ji}\right)\dot{A}_j = \frac{4\pi qc}{\Delta\zeta}\sum_{\alpha=1}^{N_p} w_\alpha\,\dot{\eta}_x^\alpha\,\rho_i(\eta_z^\alpha) \quad (52)$$

where $\pi_x^\alpha \equiv m\,\gamma_\alpha\,\dot{\eta}_x^\alpha$ and $\pi_z^\alpha \equiv m\,\gamma_\alpha(c - \dot{\eta}_z^\alpha)$, with γ_α given by (24). Note that π_x^α and π_z^α are identical to the corresponding lab-frame quantities. Once again, the spatial differencing operators are naturally combined in such a way as to correspond to central differencing.

In an infinite domain, even with a nonuniform ion density, an invariant energy integral can be constructed. In a bounded domain, since the ζ domain is moving through space, energy balance necessarily requires accounting for particle and field flux entering and leaving the domain.

A. Examples

As in Section II, we take the second-order spatial differencing and use linear finite elements for interpolation. Then, $D_{ij} = (\delta_{i+1,j} - \delta_{i-1,j})/(2\Delta\zeta)$ and $D_{ji} = -D_{ij}$, and (52) becomes

$$\ddot{A}_i + \frac{c}{\Delta\zeta}\left(\dot{A}_{i+1} - \dot{A}_{i-1}\right) = \frac{4\pi qc}{\Delta\zeta}\sum_{\alpha=1}^{N_p} w_\alpha\,\dot{\eta}_x^\alpha\,\rho_i(\eta_z^\alpha). \quad (53)$$

Again, second-order integrators are unstable [29], and we choose to implement a fourth-order Runge–Kutta scheme. We consider an under-dense plasma with $\omega_0 = 10\,\omega_p$. The initial vector potential is

$$A_x = \frac{mc^2}{q}\,a_0\exp\left(-\frac{\zeta^2}{L^2}\right)\cos(k_0\,\zeta) \quad (54)$$

with $k_p\,L = 2$ (linear resonance) and $a_0 = 1$. We take $\partial A_x/\partial\tau = 0$, which correspond to forward pulse propagation. Our boundary conditions are applied ahead of the laser pulse, i.e., the leading edge of the moving window encounters quiescent plasma, where we take the potentials and their derivatives to be zero. Our domain extends from $k_p\,\zeta_1 = -10$ to $k_p\,\zeta_2 = 70$ with 3201 grid points ($k_p\,\Delta\zeta = 0.025$). We take $c\,\Delta\tau = \Delta\zeta$ and use eight particles per cell. We use the S_2 particle shape, which gives quartic ρ_k [8, Table A.1]). In Fig. 9, we plot the dimensionless fields

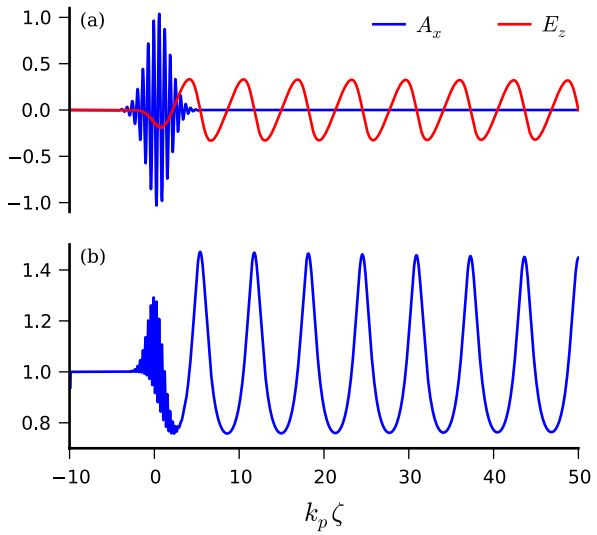

Fig. 9. Laser interacting with an under-dense plasma in the moving window at $\omega_p\,t = 60$: (a) $q\,A_x/mc^2$ (red) and $q\,E_z/mc\,\omega_p$ (blue), and (b) N_e/n_0.

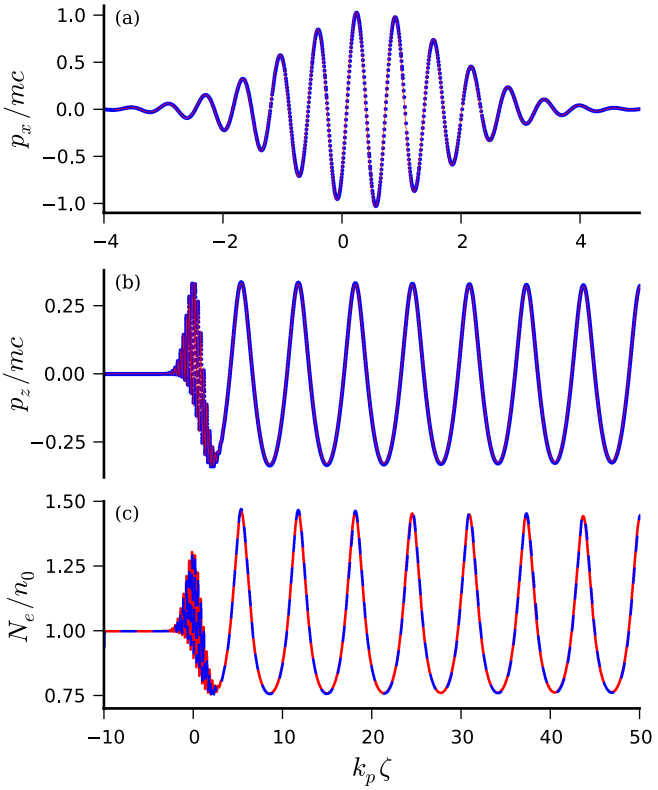

Fig. 10. Comparison of our macroparticle model (blue) to the cold fluid model (red) of laser interacting with under-dense plasma in moving window coordinates. (a) and (b) show phase space at $\omega_p t = 60$, and (c) the normalized particle density, N_e/n_0. In (a), we only show the area of nonzero x-momentum.

$q\,A_x/mc^2$, $q\,E_z/m\,c\,\omega_p$ [Fig. 9(a)], and N_e/n_0 [Fig. 9(b)] at $\omega_p\,t = 60$.

Fig. 10 shows a comparison between our macroparticle calculation and the results of a cold fluid model. The fluid model, also formulated in the moving window, uses the same spatial differencing, time integration, grid parameters and initial conditions. Fig. 10(a) shows the macroparticle momentum π_x^α (blue dots) overlaid on the transverse fluid momentum (red line). Likewise, Fig. 10(b) shows the macroparticle momentum π_z^α (blue dots) overlaid on the longitudinal fluid momentum (red line). Finally, Fig. 10(c) shows the macroparticle density (dashed blue line) and the fluid density (red line). There are no adjustable parameters in this comparison; the respective models used identical numerical parameters. Clearly, the agreement is remarkable. The macroparticle model has virtually no noise (in part due to the quartic ρ_k), even in the density. No smoothing or filtering of any kind has been applied to the macroparticle results. Note also, as in the examples of Section II, there are no signs of grid heating.

IV. Conclusion

From a discretized Lagrangian, we have derived a time-explicit energy-conserving algorithm for modeling relativistic electromagnetic kinetic laser–plasma interactions, in the 1.5-D case. Realizations of this algorithm were developed in the lab frame using both a fourth-order Runge–Kutta method and a split-step second-order Runge–Kutta/Crank–Nicolson method to integrate the system in time. We have shown that with both integrators and for two different physical scenarios, the error in energy conservation depends only on temporal discretization, as expected from a discretized Noether's theorem. A further advantage of the method was illustrated in its flexibility to accommodate a coordinate transformation by extending the formulation to moving window coordinates. Finally, all of the examples presented showed a reduction of numerical noise as compared with what would be expected from the standard PIC algorithm. The Lagrangian formulation naturally leads to the possibility of a (canonical) Hamiltonian formulation and thus the prospect of using a symplectic integrator for both the macroparticles and fields. A symplectic integrator has been demonstrated for the electrostatic case with promising computational performance [9]. The electromagnetic case leads to a significant complication as the kinetic energy depends on both coordinates and momenta, and thus the usual splitting approach fails; this is under active investigation by the authors and will be reported on in a subsequent publication.

Acknowledgment

A. B. Stamm would like to thank J. P. Reyes, J. M. Finn, M. Carrié, and D. L. Bruhwiler for their helpful conversations.

References

[1] J. M. Dawson, "Particle simulation of plasmas," *Rev. Mod. Phys.*, vol. 55, no. 2, pp. 403–447, Apr. 1983.

[2] R. W. Hockney and J. W. Eastwood, *Computer Simulation Using Particles*. New York, NY, USA: Taylor & Francis, 1988.

[3] C. K. Birdsall and A. B. Langdon, *Plasma Physics via Computer Simulations* (Plasma Physics). Bristol, U.K.: Inst. Physics Publishing, 1991.

[4] B. M. Cowan *et al.*, "Computationally efficient methods for modelling laser Wakefield acceleration in the blowout regime," *J. Plasma Phys.*, vol. 78, no. 4, pp. 469–482, 2012.

[5] A. B. Langdon, "Effects of the spatial grid in simulation plasmas," *J. Comput. Phys.*, vol. 6, no. 2, pp. 247–267, 1970.

[6] H. Okuda, "Nonphysical noises and instabilities in plasma simulation due to a spatial grid," *J. Comput. Phys.*, vol. 10, no. 3, pp. 475–486, 1972.

[7] E. Cormier-Michel, B. A. Shadwick, C. G. R. Geddes, E. Esarey, C. B. Schroeder, and W. P. Leemans, "Unphysical kinetic effects in particle-in-cell modeling of laser Wakefield accelerators," *Phys. Rev. E*, vol. 78, no. 1, pp. 016404-1–016404-17, 2008.

[8] E. G. Evstatiev and B. A. Shadwick, "Variational formulation of particle algorithms for kinetic plasma simulations," *J. Comput. Phys.*, vol. 245, pp. 376–398, Jul. 2013.

[9] B. A. Shadwick, A. B. Stamm, and E. G. Evstatiev, "Variational formulation of macro-particle plasma simulation algorithms," *Phys. Plasmas*, vol. 21, no. 5, pp. 055708-1–055708-10, 2014.

[10] F. E. Low, "A Lagrangian formulation of the Boltzmann-Vlasov equation for plasmas," *Proc. Roy. Soc. London Ser. A, Math. Phys. Sci.*, vol. 248, no. 1253, pp. 282–287, 1958.

[11] J. V. José and E. J. Saletan, *Classical Dynamics: A Contemporary Approach*. Cambridge, U.K.: Cambridge Univ. Press, 1998.

[12] B. A. Shadwick, J. C. Bowman, and P. J. Morrison, "Exactly conservative integrators," *SIAM J. Appl. Math.*, vol. 59, no. 3, pp. 1112–1133, 1999.

[13] G. Chen, L. Chacón, and D. Barnes, "An energy- and charge-conserving, implicit, electrostatic particle-in-cell algorithm," *J. Comput. Phys.*, vol. 230, no. 18, pp. 7018–7036, 2011.

[14] S. Markidis and G. Lapenta, "The energy conserving particle-in-cell method," *J. Comput. Phys.*, vol. 230, no. 18, pp. 7037–7052, 2011.

[15] G. Lapenta and S. Markidis, "Particle acceleration and energy conservation in particle in cell simulations," *Phys. Plasmas*, vol. 18, no. 7, p. 072101, 2011.

[16] P. J. Morrison, "The Maxwell-Vlasov equations as a continuous Hamiltonian system," *Phys. Lett. A*, vol. 80, nos. 5–6, pp. 383–386, 1980.

[17] A. Weinstein, "Comments on: The Maxwell-Vlasov equations as a continuous Hamiltonian system," *Phys. Lett. A*, vol. 80A, no. 4, pp. 235–236, 1981.

[18] Y. L. Klimontovich, "Relativistic transport equations for a plasma 1," *Sov. Phys. JETP*, vol. 10, no. 3, pp. 524–530, 1960.

[19] J. J. Galloway and H. Kim, "Lagrangian approach to non-linear wave interactions in a warm plasma," *J. Plasma Phys.*, vol. 6, no. 1, pp. 53–72, 1971.

[20] C. S. Gardner, "Bound on the energy available from a plasma," *Phys. Fluids*, vol. 6, no. 6, pp. 839–840, 1963.

[21] E. B. Becker, G. F. Carey, and J. T. Oden, *Finite Elements: An Introduction*, vol. 1. Englewood Cliffs, NJ, USA: Prentice-Hall, 1981.

[22] J. W. Thomas, *Numerical Partial Differential Equations: Finite Difference Methods* (Texts in Applied Mathematics), vol. 22. New York, NY, USA: Springer-Verlag, 1995.

[23] J. P. Reyes, private communication, Aug. 2013.

[24] J. C. Butcher, *The Numerical Analysis of Ordinary Differential Equations: Runge-Kutta and General Linear Methods*. New York, NY, USA: Wiley, 1987.

[25] J. Crank and P. Nicolson, "A practical method for numerical evaluation of solutions of partial differential equations of the heat-conduction type," *Math. Proc. Cambridge Philosoph. Soc.*, vol. 43, no. 1, pp. 50–67, 1947.

[26] G. Strang, "On the construction and comparison of difference schemes," *SIAM J. Numer. Anal.*, vol. 5, no. 3, pp. 506–517, 1968.

[27] M. Abramowitz and I. A. Stegun, *Handbook of Mathematical Functions*. New York, NY, USA: Dover, 1965.

[28] D. U. von Rosenberg, *Methods for the Numerical Solution of Partial Differential Equations*, (Modern Analytic and Computational Methods in Science and Mathematics), vol. 16. New York, NY, USA: Elsevier, 1969.

[29] J. P. Reyes and B. A. Shadwick, "Numerical methods for the wave equation," in *Proc. AIP Conf.*, vol. 1299. 2010, pp. 256–261.

Alexander B. Stamm (S'13) received the B.S. degree in electrical and computer engineering and the M.Eng. degree in material science and engineering from Cornell University, Ithaca, NY, USA, in 2007 and 2009, respectively. He received the M.S. degree in physics from the University of Nebraska–Lincoln, Lincoln, NE, USA, in 2011, where he is currently pursuing the Ph.D. degree in physics.

He was a recipient of the GAANN Fellowship and the IEEE Nuclear and Plasma Sciences Paul Phelps Continuing.

Bradley A. Shadwick received the B.Sc. degree in applied mathematics from the University of Western Ontario, London, ON, Canada, in 1986, and the M.Sc. degree in high-energy physics from the University of Toronto, Toronto, ON, in 1987, and the Ph.D. degree from the University of Texas at Austin, Austin, TX, USA, in 1995.

He was a Post-Doctoral Fellow with the University of California at Berkeley, Berkeley, CA, USA, and a Scientist with the Lawrence Berkeley National Laboratory, Berkeley, CA, USA, before joining the Department of Physics and Astronomy at the University of Nebraska-Lincoln, Lincoln, NE, USA, in 2007, where he is currently an Associate Professor of Physics. His current research interests include laser-plasma interactions, plasma-based particle accelerators, and computational physics.

Evstati G. Evstatiev received the B.S. and M.Sc. degrees in theoretical high-energy and nuclear physics from Sofia University, Sofia, Bulgaria, in 1995, and the Ph.D. degree from the University of Texas at Austin, Austin, TX, USA, in 2004.

He was with the Bulgarian Academy of Sciences, Sofia, from 1996 to 1997. He was a Post-Doctoral Associate with the Los Alamos National Laboratory, Los Alamos, NM, USA, from 2005 to 2008, and the University of Nebraska-Lincoln, Lincoln, NE, USA, from 2008 to 2009. He is currently a Staff Scientist with FAR-TECH, Inc., San Diego, CA, USA. His current research includes include computational plasma physics, laser-plasma interactions, magnetohydrodynamics, inertial electrostatic confinement, fluid dynamics, nonlinear dynamics, completely integrable dynamical systems, and solitons.